Electronic Supplementary Material (ESI) for Journal of Materials Chemistry A.

Supporting information for

Ultrathin RuRh@(RuRh)O_2 core@shell nanosheets as stable oxygen evolution gelectrocatalysts

Kai Wang,[1,†] Bolong Huang,[2,†] Weiyu Zhang,[1] Fan Lv,[1] Yi Xing,[1] Wenshu Zhang,[1] Jinhui Zhou,[1] Wenxiu Yang,[1] Fangxu Lin,[1] Peng Zhou,[1] Mingqiang Li,[3] Peng Gao[3,4] and Shaojun Guo[1,5]*

[1]Department of Materials Science and Engineering, College of Engineering, Peking University, Beijing 100871, China.

[2]Department of Applied Biology and Chemical Technology, The Hong Kong Polytechnic University, Hung Hom, Kowloon, Hong Kong SAR, 999077 China.

[3]Electron Microscopy Laboratory, and International Center for Quantum Materials School of Physics Peking University, Beijing 100871, China.

[4]Collaborative Innovation Center of Quantum Matter, Beijing 100871, China

[5]BIC-ESAT, College of Engineering, Peking University, Beijing 100871, China.

[†]These authors contributed equally to this work.

*Correspondence: guosj@pku.edu.cn

Methods

Chemicals. Rhodium(III) acetylacetonate (Rh(acac)$_3$, 97%) and oleylamine (OAm, 70%) were obtained from Sigma-Aldrich. Triruthenium dodecacarbonyl ($Ru_3(CO)_{12}$, 99%) was obtained from Acros. L-ascorbic acid (reagent grade, 99%) was purchased from J&K Scientifc. Ethanol and cyclohexane were supplied by Beijing Tongguang Fine Chemicals Company. Perchloric acid (GR, 70%-72%) was purchased from Sinopharm Chemical Reagent Co. Ltd (SCRC). KOH (95 %) was obtained from Aladdin. Nafion (5 wt%) was obtained from Alfa Aesar. All the chemicals were used as received without further purifcation, and all solutions were freshly prepared with water (18 MΩ/cm) by passing through an ultra-pure purification system.

Synthesis of RuRh nanosheets. The ultrathin RuRh nanosheets were synthesized as we reported.[1] ypically, 10 mg Rh(acac)$_3$, 48 mg $Ru_3(CO)_{12}$, 40 mg L-ascorbic acid and 5 mL oleylamine were added into 15 mL glass pressure vial (Synthware, P160001D) successively. Afterwards, the capped vial was placed in an oil bath and stirred at 45 °C for 60 min, and then heated to 180 °C in 20 min and kept at this temperature for 120 min before cooling down to room temperature. Then, the RhRu nanosheets were collected by centrifugation and washed three times with an ethanol/cyclohexane mixture. Then, the as-synthesized RuRh NSs was loaded onto Ketjen-300J carbon with a metal loading amount of ~20%.

Preparation of RuRh@(RuRh)O_2 core@shell nanosheets. The RuRh NSs/C was annealed in air at 286 °C for 2 h to obtain the RuRh@(RuRh)O_2 core@shell nanosheets, denoted as RuRh@(RuRh)O_2 NSs/C.

Material characterization. TEM images were obtained from a transmission electron microscope (TEM, Hitachi, HT7700) at 100 kV. The high-angle annular dark-field scanning transmission electron microscopy (HAAD-STEM) images and STEM energy-dispersive X-ray spectroscopy (STEM-EDS) elemental mapping analysis were performed on an JEOL ARM 300F transmission electron microscope at an accelerating voltage of 300 kV. Powder X-ray diffraction (XRD) patterns were collected on a Bruker D2 Phaser X-Ray Diffractometer with Cu Kα radiation ($\lambda = 1.5406$ Å) at a voltage of 40 kV and a current of 40 mA. XPS data were obtained from Thermo Scientifc Escalab 250Xi using a monochromated Al-*K*α (1486.5 eV) X-ray radiation and all the binding energies were calibrated to C 1s (284.8 eV).

Catalyst Preparation. The RuRh NSs/C and RuRh@(RuRh)O_2 NSs/C were redispersed in a solvent mixture containing deionized water, isopropanol and Nafion (D-521) (V/V/V=1/1/0.05) to form a catalyst homogeneous ink (1 mg mL^{-1}) by sonification.

Electrocatalytic Measurements. Electrochemical measurements were conducted with a CHI 760e (CH Instruments, Inc., Shanghai) in a standard three-electrode system, consisting of a glassy carbon (GC) working electrode (Pine Instruments, 0.196 cm^{-2}), saturated Ag/AgCl electrode and graphite rod used as the working, reference and counter electrodes, respectively. For each measurement, 20 μL of the catalyst ink was deposited on the GC working electrode (5 mm, 0.196 cm^2) with the catalyst metal mass loading of 20.4 ug$_{\text{metal}}$ cm^{-2}. Linear sweep voltammetries were performed in a O_2-saturated 0.1 M $HClO_4$ and 1 M KOH electrolyte with a potential range between 1.2 and 1.6 V *versus* RHE at a scan rate of 10 mV s^{-1} with iR compensations and the rotating speed fixed at 1,600 rpm. All the potentials were calibrated to the reversible hydrogen electrode (RHE). For the long-term stability test, 100 uL of the catalyst ink was dropped onto FTO conducting glass (area: 1×1 cm^2) with the metal mass loading of 20 ug$_{\text{metal}}$ cm^{-2}. Stability was measured by chronopotentiometry at constant current of 5 mA cm^{-2}.

Rotating ring disk electrod (RRDE) measurements were performed in the collection mode in a O_2-saturated 0.1 M $HClO_4$ electrolyte, wherein recording the OER was conducted on the disk electrode, the ring electrode was potentiostated at 0.9 V at which solution phase Ru^{4+} (dissolution product in acid solution) was deposited onto the ruthenized-Pt ring electrode at a diffusion control rate. The disk catalyst metal mass loading was 20.4 ug$_{\text{metal}}$ cm^{-2}, with a sweep rate 10 mV s^{-1} and a rotation rate of 1600 rpm.

Calculation Setup. All the calculations are performed by the density functional theory (DFT) within the CASTEP codes [2]. We have applied the generalized gradient approximation (GGA) in the parametrization of Perdew-Burke-Ernzerhof (PBE) for the exchange-correlation energy [3-5]. The ultrasoft pseudopotential scheme with the 380 eV cutoff energy has been chosen[6] with the algorithm Broyden-Fletcher-Goldfarb-Shannon (BFGS) for all related ground state geometry optimization[7]. The core RuRh is constructed with six-layered thickness. Meanwhile, the shell oxidation layer is modelled based on the two-layered of RuO2 (112) surface. Along the z-axis, we applied 15 Å vacuum space for all the models. Considering the DFT computational cost, the Monkhost-Pack reciprocal space integration was performed using coarse k-points with a mesh of 2×2×1 [8], which was guided by the initial convergence test. Thus, the overall total energy for each step is converged to less than 5.0x10-5 eV per atom. The Hellmann-Feynman forces on the atom were converged to less than 0.001 eV/Å.

Data availability. The data that support the plots within this paper and other finding of this study are available from the corresponding author upon reasonable request.

Supplementary Figures

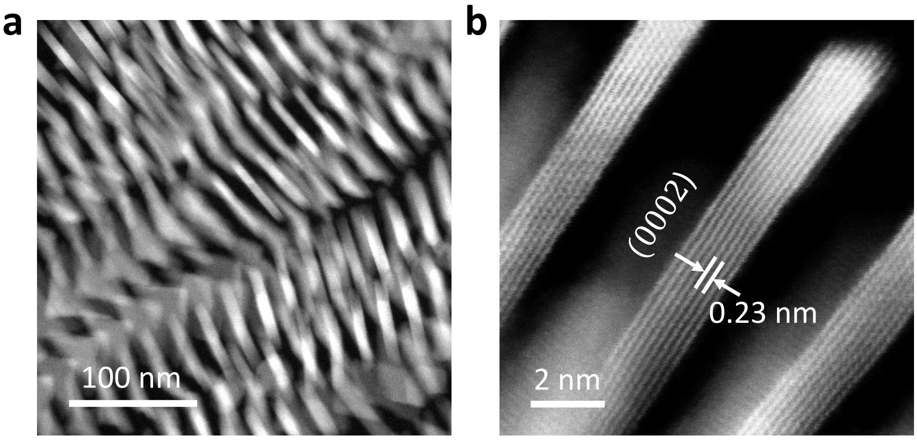

Figure S1 (a) Low magnification HAADF-STEM and (b) high magnification STEM images of triangular RuRh nanosheets perpendicular to the TEM grid.

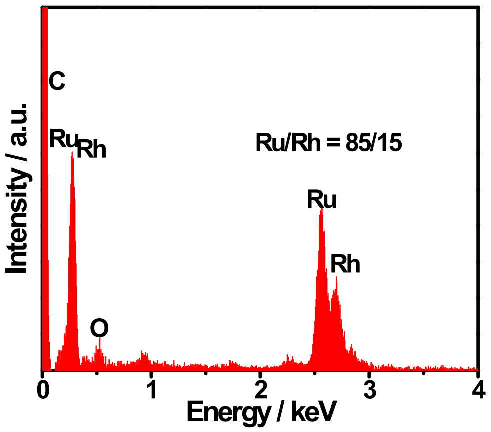

Figure S2 TEM-EDX spectrum of triangular RuRh nanosheets.

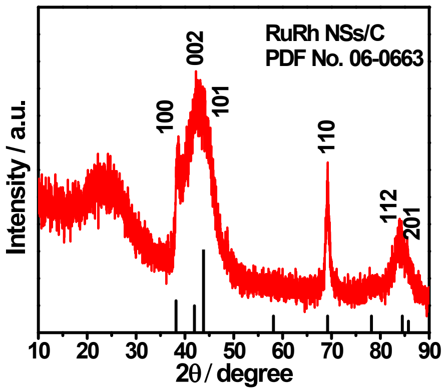

Figure S3 PXRD pattern of triangular RuRh nanosheets.

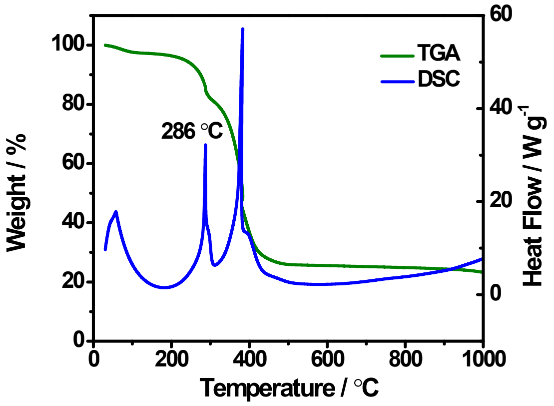

Figure S4 TGA curve and DSC curve of RuRh NSs/C.

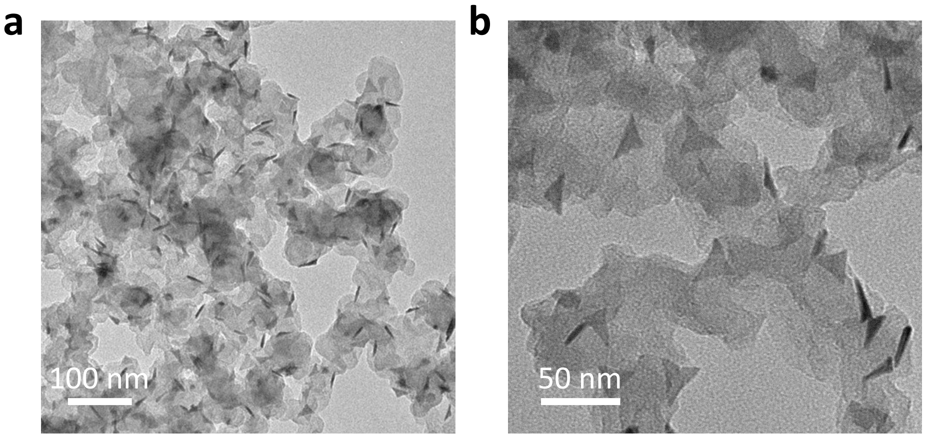

Figure S5 Representative (a) low-magnification TEM and (b) high-magnification TEM images of carbon supported triangular RuRh nanosheets.

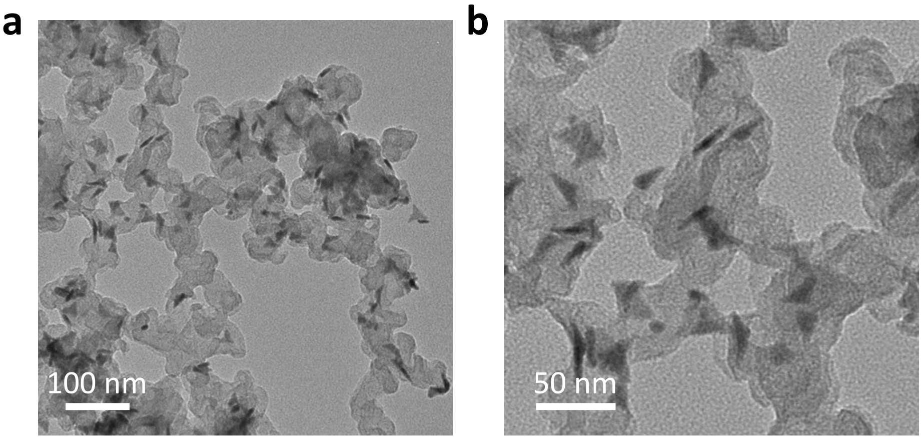

Figure S6 Representative (a) low-magnification TEM and (b) high-magnification TEM images of carbon supported triangular RuRh nanosheets after annealed in air at 286 °C for 2 h.

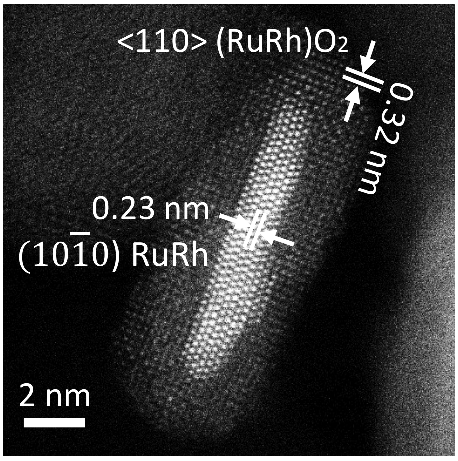

Figure S7 HAADF-STEM image of the RuRh@(RuRh)O_2 NSs.

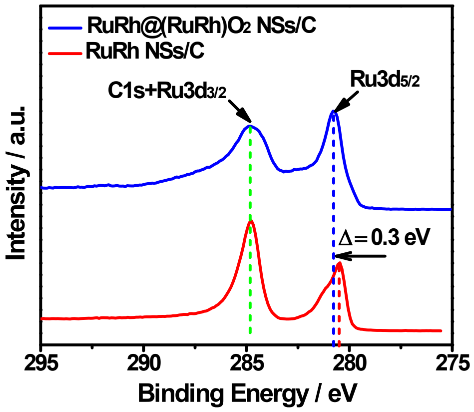

Figure S8 XPS spectra of C 1S and Ru 3d for the RuRh NSs and RuRh@(RuRh)O_2 NSs.

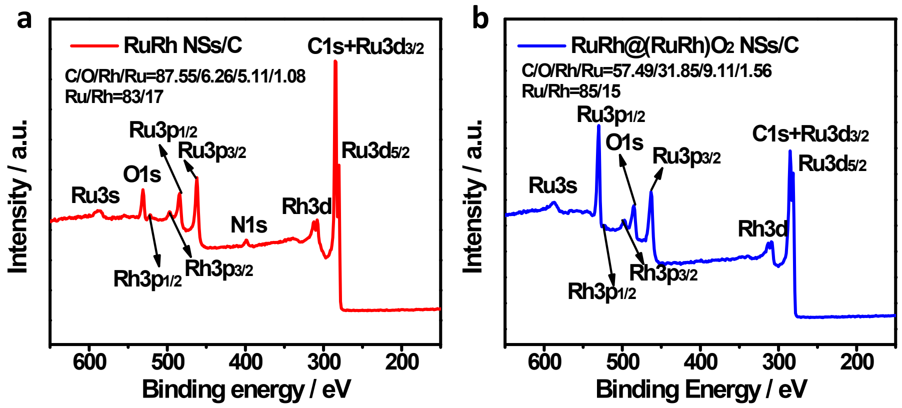

Figure S9 XPS survey spectrum of RuRh NSs/C and RuRh@(RuRh)O_2 NSs/C.

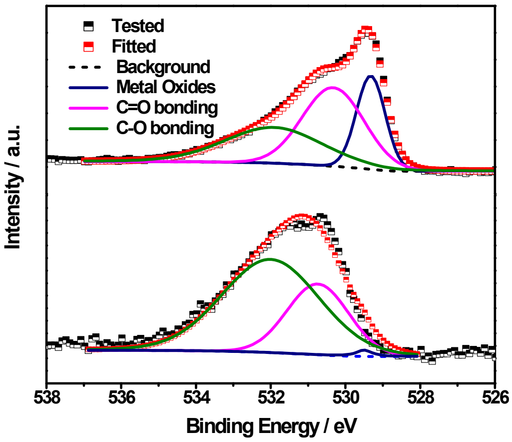

Figure S10 XPS spectra of O 1S for the RuRh NSs and RuRh@$(RuRh)O_2$ NSs.

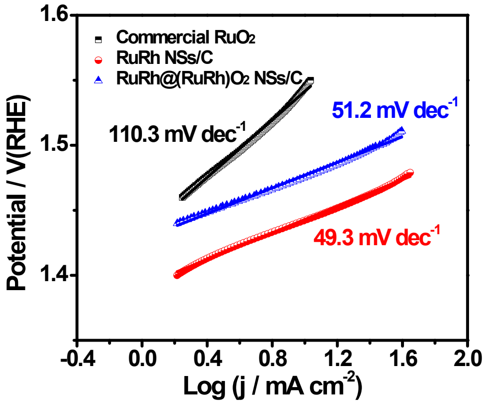

Figure S11 Tafel slope of the different catalysts.

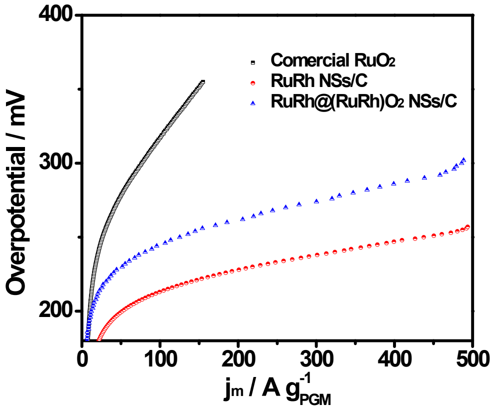

Figure S12 Mass-based activities (units of $A\ g_{PGM}^{-1}$ of RuRh NSs/C, RuRh@(RuRh)O_2 NSs/C and commercial RuO_2 in 0.1 M $HClO_4$.

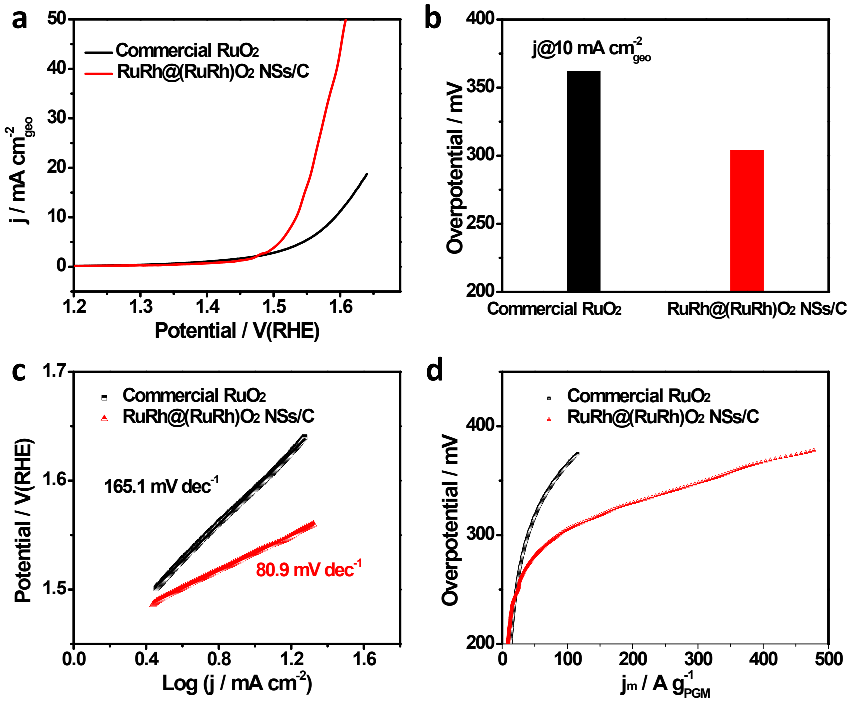

Figure S13 OER performance of RuRh@(RuRh)O$_2$ NSs/C and commercial RuO$_2$ in O$_2$-saturated 1 M KOH. (a) LSV curves, (b) overpotential at 10 mA cm^{-2}, (c) Tafel slope and (d) mass activities.

Supplementary Tables

Table S1 Summary of OER properties of state-of-the-art electrocatalysts reported in literatures in acid.

Catalyst	Electrolyte	Noble Metal loading ug_{metal} cm^{-2}	η @10 mA cm^{-2}	Tafel slope mV dec^{-1}	Reference
RuRh@$(RuRh)O_2$ NSs/C	0.1 M $HClO_4$	20.4	245 mV	51.2	***This work***
Ruthenium Oxide Nanosheets	0.1 M $HClO_4$	200	255 mV	38	Adv. Energy Mater. 2019, 9, 1803795
IrNiCo PHNCs	0.1 M $HClO_4$	10.0	303 mV	53.8	Adv. Mater. 2017, 29, 1703798
Channel-Rich RuCu NSs	0.05 M H_2SO_4 0.5 M H_2SO_4	/	240 mV 236 mV	52 41	Angew. Chem. Int. Ed. 2019, 58, 13983
Ru@IrOx	0.05 M H_2SO_4	51.0	282 mV	69.1	Chem 2019, 5, 445.
RuO_2-NWs@g-CN	0.5 M H_2SO_4	~61.2	250 mV	52	ACS Appl. Mater. Interfaces 2016, 8, 28678
Iridium Nanosheets	0.5 M H_2SO_4	135.9	240 mV	49	J. Am. Chem. Soc. 2018, 140, 12434
Surface-clean 3D Ir	0.1 M $HClO_4$	11.5	276 mV	40.8	Nano Lett. 2016, 16, 4424
Ir_3Cu Metallic Aerogels	0.1 M $HClO_4$	~25.5	298 mV	47.4	ACS Energy Lett. 2018, 3, 2038
Free-Standing Two-Dimensional Ru Nanosheets	0.5 M H_2SO_4	102.0	η @1 mA cm^{-2} 260 mV	54	ACS Catal. 2016, 6, 1487
Iridium−Tungsten Alloy Nanodendrites	0.1 M $HClO_4$	10.2	η @1.6 mA cm^{-2} 300 mV	56.6	ACS Cent. Sci. 2018, 4, 1244
Co-Doped RuIr	0.1 M $HClO_4$	~51.0	235 mV	66.9	Adv. Mater. 2019, 31, 1900510
Mn-doped RuO_2 Nanocrystals	0.5 M H_2SO_4	~275	158 mV	42.9	ACS Catal. 2020, 10, 1152
Ru_3Ni_3 NAs	0.5 M H_2SO_4	102.0	252 mV	45.8	iScience, 2019, 11, 492
$IrNiO_x$/Meso-A TO	0.05 M H_2SO_4	10.2	η @4.6 mA cm^{-2} 280 mV	/	Angew. Chem. Int. Ed. 2015, 54, 2975

Table S2 RRDE results analysis of all samples. The ring efficiency was 38 %.

	Disk current at 1.53 V (mA)	Ring current at 1.53 V (uA)	Corrected ring current at 1.53 V (uA)	Corrected ring current / Disk current (%)
Commercial RuO_2	1.24	0.30	0.79	0.064
RuRh NSs/C	3.30	91.97	$2.4*10^2$	7.3
RuRh@$(RuRh)O_2$ NSs/C	2.23	0.41	1.1	0.049

Table S3 ICP-MS results obtained from the electrolyte after chronopotentiometry experiment at 5 mA cm^{-2}.

	Ru(ng cm^{-2} s^{-1})	Rh(ng cm^{-2} s^{-1})
Commercial RuO_2	0.030	/
RuRh NSs/C	4.0	0.18
RuRh@$(RuRh)O_2$ NSs/C	0.060	0.00076

References

[1] Y. Xing; K. Wang; N. Li; D. Su; W. T. Wong; B.L. Huang; S. J. Guo, Ultrathin RuRh Alloy Nanosheets Enable High-Performance Lithium-CO_2 Battery. *Matter* 2020, https://doi.org/10.1016/j.matt.2020.02.020.

[2] S. J. Clark; M. D. Segall; C. J. Pickard; P. J. Hasnip; M. J. Probert; K. Refson; M. C. Payne, First Principles Methods Using Castep. *Zeitschrift Fur Kristallographie* 2005, 220 (5-6), 567-570.

[3] J. P. Perdew; K. Burke; M. Ernzerhof, Generalized Gradient Approximation Made Simple. *Phys. Rev. Lett.* 1996, 77 (18), 3865-3868.

[4] P. J. Hasnip; C. J. Pickard, Electronic Energy Minimisation with Ultrasoft Pseudopotentials. *Comput. Phys. Commun.* 2006, 174 (1), 24-29.

[5] J. P. Perdew; J. A. Chevary; S. H. Vosko; K. A. Jackson; M. R. Pederson; D. J. Singh; C. Fiolhais, Atoms, Molecules, Solids, and Surfaces: Applications of the Generalized Gradient Approximation for Exchange and Correlation. *Phys. Rev. B* 1992, 46 (11), 6671-6687.

[6] D. Vanderbilt, Soft Self-Consistent Pseudopotentials in a Generalized Eigenvalue Formalism. *Phys. Rev. B* 1990, 41 (11), 7892-7895.

[7] J. D. Head; M. C. Zerner, A Broyden—Fletcher—Goldfarb—Shanno Optimization Procedure for Molecular Geometries. *Chem. Phys. Lett.* 1985, 122 (3), 264-270.

[8] M. I. J. Probert; M. C. Payne, Improving the Convergence of Defect Calculations in Supercells: An Ab Initio Study of the Neutral Silicon Vacancy. *Phys. Rev. B* 2003, 67 (7), 075204.